Surface Structures and Phase Transitions at the Au(100)−Br Interface: pH and CO Effects

B. B. Blizanac,[†] C. A. Lucas,[‡] M. E. Gallagher,[‡] P. N. Ross,[†] and N. M. Marković*,[†]

Materials Sciences Division Lawrence Berkeley National Laboratory, University of California, Berkeley, California 94720, and Oliver Lodge Laboratory, Department of Physics, University of Liverpool, Liverpool, L69 7ZE United Kingdom

Received: November 27, 2003; In Final Form: January 20, 2004

The surface reconstruction of Au(100) and the formation of an ordered commensurate c($\sqrt{2} \times 22\sqrt{2}$)R45° adlayer of Br ($Br_{ad}$) have been studied by a combination of electrochemical (EC) and surface X-ray scattering (SXS) measurements. Emphasis is placed on linking the microscopic structural information concerning the Br_{ad} adlayer to the voltammetric and other macroscopic electrochemical responses, including using the rotating ring disk electrode (RRDE) measurements for determining the surface coverage by Br_{ad}. It is found that the potential-induced hexagonal ("hex") to (1 × 1) transition of the Au surface coincides with Br^- adsorption and occurs faster in solutions containing Br^- anions than in Br^--free solutions. In agreement with previous SXS results, in acid solutions, Br_{ad} forms a c($\sqrt{2} \times 2\sqrt{2}$)R45° structure at around 0.15 V. However, no ordered structures of Br_{ad} are observed in alkaline solution, although the cyclic voltammetry indicates that the order structure should be present at 0.12 V. Absence of an ordered Br_{ad} adlayer in alkaline solution is attributed to competitive adsorption between Br_{ad} and OH_{ad}. To probe the role of OH_{ad} on the ordering of the bromide adlayer, coadsorbed OH_{ad} is consumed in an electrochemical reaction in which strongly adsorbed OH_{ad} is removed from the surface by a relatively weakly adsorbed reactant, viz. CO_{ad}. Under such experimental conditions, we found that (i) in acid solution the c($\sqrt{2} \times 2\sqrt{2}$)R45° structure develops/disappears more rapidly than in CO-free solution and (ii) in alkaline solution the c($\sqrt{2} \times 2\sqrt{2}$)R45° structure is formed in exactly the same potential region as in acid solution. We propose that the continuous removal of OH_{ad} in the Langmuir−Hinshelwood reaction ($CO_{ad} + OH_{ad} = CO_2 + H^+ + e^-$) may stabilize the c($\sqrt{2} \times 2\sqrt{2}$)R45° structure in both acid as well as alkaline media.

1. Introduction

The interaction of specifically adsorbed anions with fcc metal surfaces has been a subject of intense theoretical and experimental interest, for review see refs 1−4. In the past decade, emphasis has been placed on linking the microscopic structural information concerning the anion adlayer structures to the thermodynamics and other macroscopic electrochemical responses at the metal−anion interface. Whereas information regarding macroscopic properties has come from classical electrochemical techniques,[2,5] a new insight into the structural changes that occur on the atomic level has been obtained from the application of in situ scanning tunneling microscopy (STM)[1,3,6−9] and surface X-ray scattering[2,3,10−15] techniques. Of the various systems studied, halide adsorption on gold single crystals has been of central significance in surface electrochemistry. The interest in such adlayers is multifaceted, including extraction of real-space structures of halides as a function of potential[1,3,4] and halide-induced changes in the gold structure (surface restructuring, i.e., arrangements of metal surface atoms which differ from the ideal bulk-termination structure)[1,3,4] as well as the influence of anions on the electrochemical reactivity of gold.[16]

In examining the Au(*hkl*)−Br system, the Brookhaven group found that each low-index Au surface exhibits an interesting sequence of potential-induced phase transitions associated with the formation of ordered bromide adlayer (Br_{ad}) phases.[12−15] For example, unlike the continuous electrocompression of the bromide adlayer observed on Au(111)[12,15,17] in acid solution, the bromide adlayer on Au(100) has been observed to undergo a commensurate−incommensurate transition where a commensurate c($\sqrt{2} \times 2\sqrt{2}$)R45° structure transforms continuously to an incommensurate c($\sqrt{2} \times$ p)R45° structure. The potential-dependent phase behavior and the Br_{ad} compressibility were rationalized by the adsorbate−adsorbate interactions rather than the halide−substrate interactions. In contrast to acid media, however, there are no complementary structural studies of the Au(*hkl*)−halide interface in alkaline solution.

Recently, it has been reported that halide adsorption shifts the "equilibrium" potential of the Au "hex" ↔ (1 × 1) transition to lower values, supportive of a substantial covalent contribution to the Au(*hkl*)−halide bond.[1,3] Similarly, an example of halide-induced "lifting" of the reconstruction was observed by SXS for the Au(100) electrode in chloride-containing solution. In this case, specific adsorption of Cl^- shifted the lifting of Au reconstruction to less positive potentials and also enhanced the conversion dynamics.[16] Besides enabling us to establish the effect of Cl_{ad} on the reconstruction, the latter study also shed some light on the energetics of the interaction of adsorbed oxygenated species (hereafter denoted as OH_{ad}) and Cl_{ad} with the Au surface in acid electrolytes. Although the results summarized in ref 16 demonstrated that there is a strong competition between Cl_{ad} and OH_{ad} for the surface sites, the details of this competition as well as the structural information

* To whom correspondence should be addressed. E-mail: nmmarkovic@lbl.gov.
[†] Materials Sciences Division Lawrence Berkeley National Laboratory, University of California, Berkeley.
[‡] University of Liverpool.

10.1021/jp037623u CCC: $27.50
Published on Web 04/02/2004

for halide adlayers on an OH_{ad}-free surface are unclear, in part due to the difficulty of removing OH_{ad} from the surface. The elucidation of this competition, from the standpoint of both ordering of halide adlayers on metal electrodes as well as electrochemical reactivity, is as significant in model systems as in systems of practical importance.

In this paper, we examine further the Au−halide system in both acidic and basic media. The Au(100)−Br_{ad} system is chosen because it gives insight into the relationship between the potential-dependent surface coverage of Br_{ad} ($\Theta_{Br_{ad}}$), established in this work by the rotating ring-disk technique with a Au(100) single crystal in the disk position, and the thermodynamic/dynamic stability of both the "hex" ↔ (1 × 1) transition of the gold surface as well as the formation of the c($\sqrt{2} \times 2\sqrt{2}$)R45° Br_{ad} structure. Included in these experiments are the effects of competitive adsorption between OH_{ad} and Br_{ad}, both on the Au surface reconstruction and on the ordering/disordering of the Br_{ad} adlayer structures. The role of OH_{ad} was established by monitoring the microscopic interface structures of Br_{ad} during the consumption of OH_{ad} in an electrochemical reaction in which strongly adsorbed OH_{ad} is removed from the surface by a relatively weakly adsorbed reactant, in this case CO_{ad}.

2. Experimental Section

2.1. Electrochemical Measurements. The pretreatment and assembly of the Au(100) single crystal (0.283 cm^2) in a RRDE configuration was fully described previously,[18] e.g., the crystal was flame annealed in a propane flame and cooled in an Ar atmosphere before being mounted in the RRDE setup. Subsequently, the electrode was transferred into a thermostated standard three compartment electrochemical cell and immersed into Ar-purged (Ar: Bay Gas Research Purity) electrolytes: 0.1 M $HClO_4$ (EM science Suprapure), 0.1 M $HClO_4$ plus Br^- (KBr, Fluka Microselect), 0.1 M KOH (Aldrich Semiconductor Grade), and 0.1 M KOH plus Br^- at room temperature (298 K) under potentiostatic control. The ring-shielding property of the RRDE was employed to assess the mass flux of Br^- from and to the Au(100) disk electrode. In these experiments, the ring electrode is potentiostated such that Br^- oxidation to Br_2

$$Br^- \rightarrow (1/2)Br_2 + e^- \ (E^\circ = 0.847 \text{ V vs SCE}) \qquad (1)$$

occurs under diffusion control at +1.08 V. At this potential, 99% of the conversion takes place without further oxidation to HBrO and the formation of three bromide ions.[19] In the absence of Br-adsorption/desorption on the disk electrode, the measured ring current represents the diffusion-limited conversion of Br^- to Br_2 and is referred to as the unshielded ring current, $i_r^{\%}$. If Br^- is adsorbed on the Au(100) disk electrode, its concentration in the vicinity of the electrode is reduced so that the ring current decreases from its $i_r^{\%}$ value and vice versa; for details, see ref 19. In the CO experiments, the electrolyte was equilibrated for 10 min with CO gas (Air Products 5N8 purity) at potentials close to the hydrogen evolution region. The reference electrode was a saturated calomel electrode (SCE) separated by a closed electrolyte bridge from the working electrode compartment in order to avoid chloride contamination. All potentials, therefore, refer to that of the SCE. The collection efficiency of the RRDE setup was $N = 0.22 \pm 5\%$.

2.2. SXS Measurements. The general experimental procedure used in X-ray diffraction measurements of electrochemical systems has been described in detail in previous articles.[4,11,20,21] The crystal (miscut <0.1°) was prepared as for the electrochemical measurements and then transferred into the X-ray electrochemical cell. The cell was mounted at the center of a four-circle Huber goniometer on beamline 7−2 at the Stanford Synchrotron Radiation Laboratory (SSRL), utilizing a 10 keV incident X-ray beam, defined by slits to be a 1 mm × 1 mm spot at the sample. Diffracted X-rays were measured by a Ge solid-state detector after passing through a Soller slit which defined an in-plane resolution of ca. 0.005 $Å^{-1}$. The crystal was indexed to the conventional fcc unit cell for Au. The adsorption of CO was studied by purging the outer shell of the X-ray cell with CO (99,999% purity) which was then able to diffuse through the polypropylene film trapping the electrolyte and saturate the solution. Further experimental details can be found in the refs 16 and 22.

3. Results and Discussion

3.1. Br Surface Coverage and Adlayer Structures. A detailed description of the structure and phase behavior of Br_{ad} adlayers at the Au(100)−electrolyte interface in acid solutions (viz., the adlayer symmetry, the nearest neighbor spacing within the ordered adlayer, etc.) is provided in a review by Magnussen.[3] No attempt is made here to repeat this analysis. For our purposes, however, some of the well-established EC−SXS results in acid solutions will be presented to provide a basis, when combined with new EC−SXS results in alkaline solution, for understanding the pH effects on both the thermodynamic stability of the "hex" phase as well as on the formation of the c($\sqrt{2} \times 2\sqrt{2}$)R45° bromide structure.

3.1.1. Acid Solution. Figure 1 shows a representative cyclic voltammetric response of Au(100) in 0.1 M $HClO_4$ + 10^{-3} M Br^-. The voltammograms are obtained under conditions that correspond closely to those utilized in the SXS experiments; that is, to ensure the complete reconstruction of the electrode surface (the "hex" phase), prior to recording the first current−potential response in solution containing 10^{-3} M Br^-, the electrode potential was held at −0.4 V (the immersion potential) for 10 min. Upon sweeping the potential positively from −0.45 V, there are several voltammetric features that signal the occurrence of specific surface processes. For example, lifting of the "hex" reconstruction and the formation of the (1 × 1) phase is clearly seen on the first cycle as a pronounced current peak at −0.15 V, labeled here as P_T. A schematic model of the hexagonal (the so-called "5 × 20" reconstruction) transition to a square-planar substrate is depicted in Figure 1. For further details on reconstruction phenomena at the metal−electrolyte interface, readers are referred to Kolb's review.[1] At more positive potentials, the substrate reconstruction peak at −0.15 V is followed first by a very sharp peak at 0.15 V (labeled as P_1) and then by a smaller peak that is centered at 0.5 V (peak P_2). As demonstrated previously[1,9,13,14,23] and discussed in detail below, whereas the voltammetric feature at around 0.15 V can be identified as arising from the formation of the c($\sqrt{2} \times 2\sqrt{2}$)-R45° structure (with a fractional coverages of Br_{ad}, $\Theta_{Br_{ad}} = 0.5$ ML), the voltammetric feature at 0.5 V represents a commensurate-incommensurate transition in the Br_{ad} adlayer structures. The subsequent potential scan in the negative direction reflects the voltammetric response on the (1 × 1) surface; so does the second scan (red curve) in the positive direction if the potential was not held at −0.45 V. Figure 1 shows that in the second scan the electrochemical fingerprint of the Au "hex" ↔ (1 × 1) reconstruction is not observed at −0.15 V, indicating that the (1 × 1) → "hex" potential-induced transition in bromide media is sluggish under relatively fast (50 mV/s) potentiodynamic conditions.

Having identified the cyclic voltammetric features of the Au(100)−Br system, it is interesting to determine the potential-

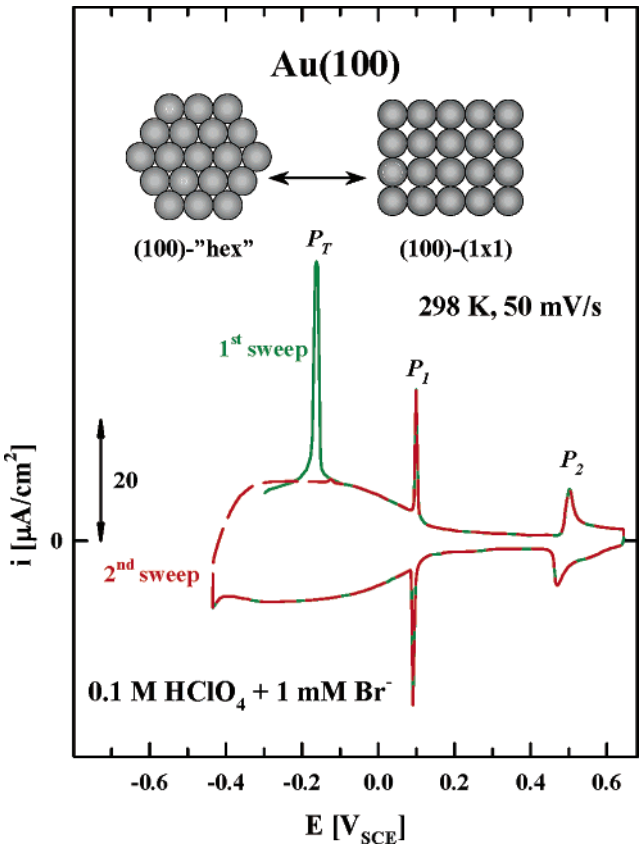

Figure 1. Cyclic voltammograms for Au(100) in 0.1 M $HClO_4$ containing 1×10^{-3} M Br^- at 50 mV/s and under a rotation rate of 900 rpm, starting with a flame annealed "hex" structure at −0.45 V. In the first potential sweep (green curve), the "hex" ↔ (1 × 1) transition, labeled as P_T, is seen at −0.15 V. A simple schematic model of a hexagonal (the so-called "5 × 20" reconstruction) to square-planar substrate structural transitions of the Au(100) surface is depicted in the upper part of Figure 1. The current sharp peaks, labeled as P_1 and P_2, are due to structural transitions within the Br_{ad} adlayer, i.e., the formation of a $c(\sqrt{2} \times 2\sqrt{2})R45°$ structure with $\Theta_{Br_{ad}} = 0.5$ ML (peak P_1) as well as a commensurate-incommensurate $c(\sqrt{2} \times 2\sqrt{2})R45° \leftrightarrow c(\sqrt{2} \times p)R45°$ transition (peak P_2). In the second sweep (red curve), lifting of the "hex" reconstruction during the positive scan is not seen; only the Br_{ad} transition peaks (P_1 and P_2) are observed at 0.18 and 0.5 V.

dependent surface coverage of Br_{ad} (the $E-\Theta_{Br_{ad}}$ curve) in solution containing 10^{-3} M Br^-. Although the ring-shielding properties of the RRDE can be used to assess the fractional coverages of Br_{ad} without interference from double layer effects, the assessment of $\Theta_{Br_{ad}}$ in solution containing 10^{-3} M Br^- is not possible because in shielding experiments the solution concentration of Br^- must be below 1×10^{-4} M.[19] To overcome this limitation, we developed a methodology that allows the $E-\Theta_{Br_{ad}}$ curve even to be derived for high Br^- concentration. Two assumptions are used: (i) the shape of the $E-\Theta_{Br_{ad}}$ curve is concentration independent and (ii) a rigid shift in the E vs $\Theta_{Br_{ad}}$ curve to lower potential is possible by an amount equal to the concentration-dependent position of the P_1 peak which marks a surface coverage of $\Theta_{Br_{ad}} = 0.5$ ML. Similarly to the approach used for the Pt(100)−Br system,[24] the true "adsorption isotherm" of Br_{ad} on Au(100) in 8×10^{-5} M Br^- is established by utilizing RRDE measurements. The qualitative correspondence between ring and disk currents (not shown, for details see ref 19) is evaluated quantitatively in terms of the E vs $\Theta_{Br_{ad}}$ relationship and summarized in Figure 2b. As is common for specific adsorption of anions,[5,19,25−28] in solution containing 8×10^{-5} M Br^-, the $E-\Theta_{Br_{ad}}$ curve exhibits the classical "S"

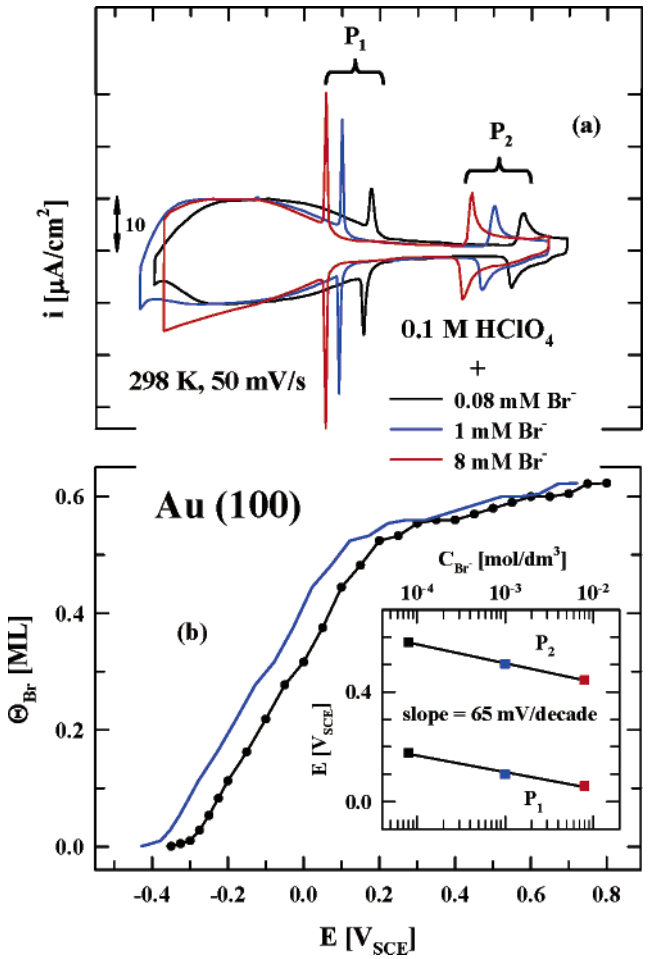

Figure 2. (a) Cyclic voltammograms (second sweeps) for Au(100) in 0.1 M $HClO_4$ containing 8×10^{-5} M Br^-, 1×10^{-3} M Br^-, and 8×10^{-3} M Br^- at 50 mV/s and under a rotation rate of 900 rpm. Note, at 50mV/s the second scan reflects the electrochemical behavior of a Au-(100)−(1 × 1) surface. As in Figure 1, peaks labeled P_1 and P_2 are due to structural transitions within the Br_{ad} adlayer. (b) Black curve, the fractional coverages of Br_{ad} on Au(100) as a function of potential (the $E-\Theta_{Br_{ad}}$ curve), assessed from potentiostatic ring shielding experiments (900 rpm) in 0.1 M $HClO_4$ containing 8×10^{-5} M Br^-; Blue curve, the derived fractional coverages of Br_{ad} on Au(100) in 0.1 M $HClO_4$ containing 1×10^{-3} M Br^- (for details see text). Insert: Concentration-dependent position of the Br_{ad} transition peaks, labeled in (a) as P_1 and P_2 peaks.

shape; that is, initially, the bromide surface concentration changes only slowly with potential then a steep rise in fractional coverage is observed, followed by a third regime of slow increase where the adlayer packing density is close to saturation. The concentration-dependent position of P_1 peak ($dE/d \log c_{Br^-}$) was acquired from 0.1 M $HClO_4$ containing three different concentrations of Br^-, i.e., 8×10^{-5} M, 1×10^{-3} M, and 8×10^{-3} M Br^-. Stable cyclic voltammograms (second sweeps) of Au(100) in these three electrolytes under a rotation rate of 900 rpm are summarized in Figure 2a. Clearly, by increasing the Br^- concentration, the position of the P_1 peaks is shifted to less positive values, by an amount equal to the difference in Br^- concentration, which is $dE/d \log c_{Br^-} = 65$ mV (see the insert of Figure 2). In agreement with refs 13 and 23, the same slope is also obtained for the P_2 peaks. Closely following the methodology described above, the derived $E-\Theta_{Br_{ad}}$ curve in the presence of 10^{-3} M Br^- (Figure 2b) is, in fact, the adsorption isotherm obtained in solution containing 8×10^{-5} M Br^- shifted in the negative direction by 78 mV, i.e., by the value required to satisfy the concentration-dependent position of the transition

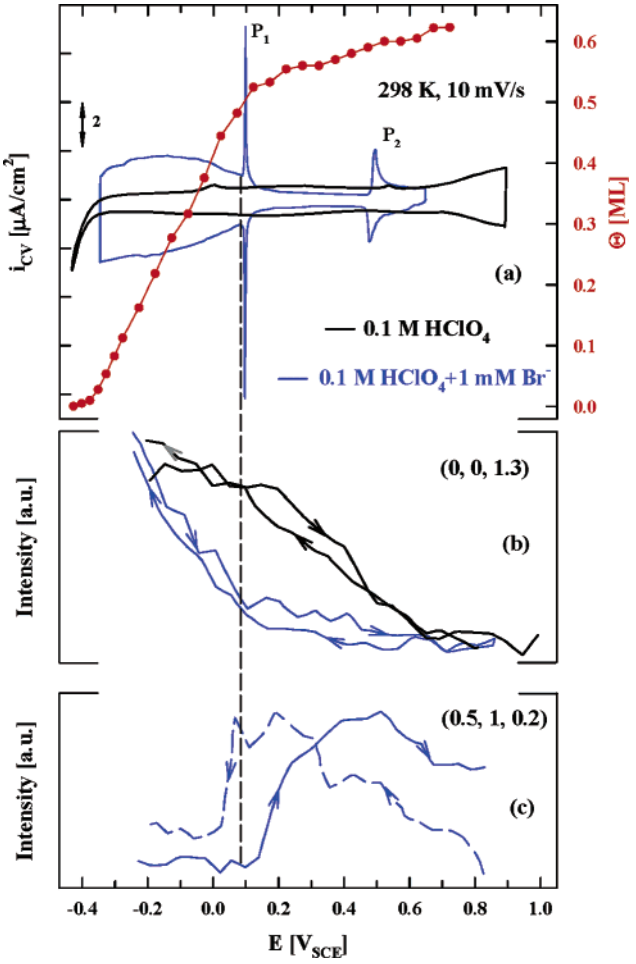

Figure 3. (a) Cyclic voltammograms (second and consecutive sweeps) for Au(100) in 0.1 M $HClO_4$ (black curve) and 0.1 M $HClO_4 + 10^{-3}$ M Br^- (blue curve) at 10mV/s. As in Figure 1, peaks labeled P_1 and P_2 are due to structural transitions within the Br_{ad} adlayer. For discussion purposes, the $E-\Theta_{Br_{ad}}$ curve shown in Figure 2 for 10^{-3} M Br^- is also included (red curve). (b) Corresponding XRV measurements (2 mV/s) at (0, 0, 1.3), a position on the specular CTR. (c) XRV measurements (2 mV/s) at (0.5, 1, 0.2), a position sensitive to scattering from the c($\sqrt{2} \times 2\sqrt{2}$)R45° structure of Br_{ad}.

peak for the formation of the c($\sqrt{2} \times 2\sqrt{2}$)R45° structure with $\Theta_{Br_{ad}} = 0.5$ ML.

Figure 3 summarizes representative electrochemical (Figure 3a) and SXS results (Figure 3, parts b and c) for the Au(100) electrode in 0.1 M $HClO_4$ with and without Br^-. The cyclic voltammetry in Br^- -free solution shows characteristic "double layer"-like peaks, in addition to a pure capacitive component. Small voltammetric features signal the occurrence of the specific adsorption of anions (ClO_4^-, Cl^-) and OH^- [16] even in the "double-layer" potential region. As discussed recently,[16] the adsorption of these anions causes the reconstructed Au surface to transform to the (1 × 1) phase at rather negative potentials. The potential-dependence of the X-ray scattering intensity (so-called X-ray voltammetry, XRV) at the (0, 0, 1.3) reciprocal space position in 0.1 M $HClO_4$ is shown in Figure 3b. In agreement with ref 16, although a reversible change in scattering intensity is observed at the specular crystal truncation road (CTR) position, at the reconstruction-sensitive reciprocal space position (XRV is not shown, for details see ref 16), there is hysteresis as the potential is cycled. Given that the specular CTR is only sensitive to the density change at the surface, it was proposed that, although the specific adsorption of anions acts to catalyze the mobility of gold surface atoms, the formation

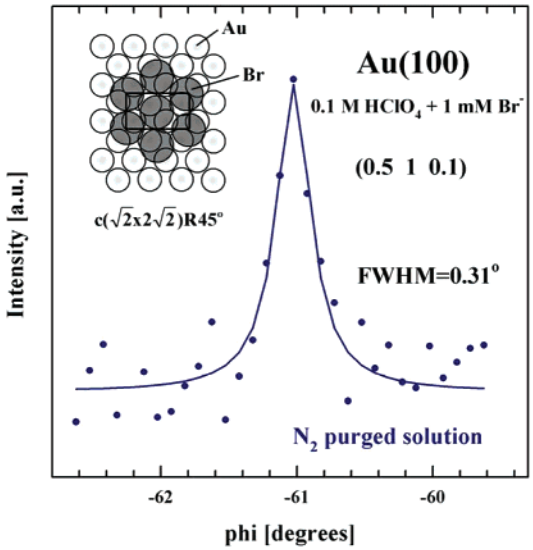

Figure 4. Rocking scans through the (0.5, 1, 0.1) reciprocal lattice position, where scattering from the commensurate c($\sqrt{2} \times 2\sqrt{2}$)R45° structure of the Br_{ad} adlayer in 0.1 M $HClO_4 + 10^{-3}$ M Br^- is observed. The solid lines are fits of a Lorentzian line shape to the data which gives coherent domain size for the c($\sqrt{2} \times 2\sqrt{2}$)R45° structure of ≈150 Å. Also shown is a schematic picture of the c($\sqrt{2} \times 2\sqrt{2}$)R45° unite cell.

of uniform "hex" domains is not enhanced by this movement. Similarly to the effect of Cl_{ad} on the "hex" ↔ (1 × 1) transition,[16] the specific adsorption of Br^- (see the $E-\Theta_{Br_{ad}}$ curve in Figure 3a) shifts the equilibrium potential of the "hex" → (1 × 1) transition to less positive values (from Figure 3b ca. 0.3 V) relative to the Br^--free solution. Furthermore, Br_{ad} can enhance the conversion dynamic; that is, in the presence of Br^-, a sharp lifting of the reconstruction is observed in Figure 3b. These results support the previous suggestion that the sharp lifting of the "hex" phase is controlled by the strong adsorption of halide anions.[1,11,16] Further inspection of Figure 3, parts a and b, reveals that the "hex" → (1 × 1) transition is completed at ca. 0.1 V or, based on the corresponding (0.5, 1, 0.2) X-ray intensity in Figure 3c, just before the formation of the c($\sqrt{2} \times 2\sqrt{2}$)R45° Br_{ad} adlayer. A rocking scan through the (0.5 1 0.1) position is shown in Figure 4 together with the fit of a Lorentzian line shape to the data. From the width of this peak and from the similar fits to other c($\sqrt{2} \times 2\sqrt{2}$)R45° reflections, a coherent domain size of 150 Å for the Br_{ad} adlayer was deduced. The derived structure model is shown schematically as an insert of Figure 4, which is consistent with $\Theta_{Br_{ad}} = 0.5$ ML. From Figure 3c and refs 9, 13, 14, and 23, the potential induced formation of the c($\sqrt{2} \times 2\sqrt{2}$)R45° structure is mirrored by the appearance of a sharp voltammetric feature at around 0.15 V (Figure 3a). The corresponding potential-dependent intensity of the c($\sqrt{2} \times 2\sqrt{2}$)R45° diffraction peak, shown in Figure 3c, is in perfect agreement with previous SXS[13,14] and STM[9] results. In particular, Figure 3c shows that the c($\sqrt{2} \times 2\sqrt{2}$)R45° structure is stable in the potential region where the corresponding increase in the fractional Br_{ad} coverage is rather small, i.e., in Figure 3a from 0.5 ML at 0.15V to 0.58 ML at 0.5 V. Further adsorption of Br_{ad} leads to the transition from a commensurate c($\sqrt{2} \times 2\sqrt{2}$)R45° structure to a uniaxially incommensurate c($\sqrt{2} \times$ p)R45° structure, ($2\sqrt{2} \geq p \geq 2.5$). As the potential-dependent phase behavior and coverage of Br adlayers on Au(100) is discussed in detail by the Brookhaven group, in this work, SXS results will not be shown for $E > 0.5$ V. We note, however, that Wandlowski et al.[13] described the incommensurate phase by an atomic model in which uniform compression occurs within

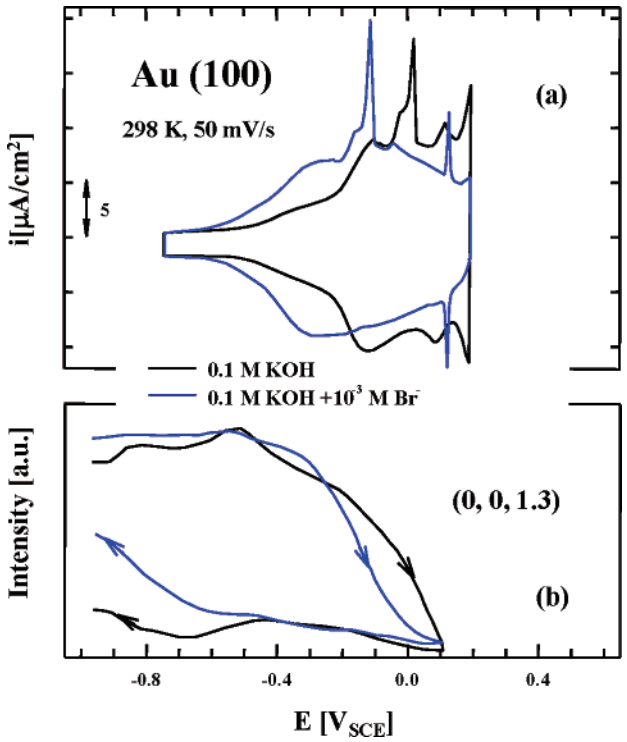

Figure 5. (a) Cyclic voltammograms (second and consecutive sweeps) for Au(100) in argon purged 0.1 M KOH (black curve) and 0.1 M KOH + 10^{-3} M Br^- (blue curve) at 50 mV/s. Lifting of the "hex" reconstruction during the positive scan is indicated by sharp current peaks around +0.1 V and −0.1 V in 0.1 M KOH and 0.1 M KOH + 10^{-3} M Br^-, respectively. (b) Corresponding XRV measurements (2 mV/s) at (0, 0, 1.3), a position on the specular CTR.

the layer. In the cyclic voltammetry of Figure 3, this transition is mirrored by the appearance of an irreversible peak at 0.5 V (peak P_2). From Figure 3a, the surface coverage of Br_{ad} increases from 0.57 ML at ≈0.5 V to 0.61 ML at 0.7 V. This is close to saturation coverage based on the van der Waals radius of Br relative to the surface density of gold atoms.

3.1.2. Alkaline Solution. As for the acid solution, in alkaline solution, we are interested in comparing the voltammetric response of the Au(100)−Br system to the corresponding SXS measurements. In a solution free of Br^-, a significant voltammetric feature of Au(100) in 0.1 M KOH (Figure 5a) is the sharp peak at −0.15 V. This peak was suggested to be associated with the potential-induced adsorption of OH^- and lifting of the Au reconstruction.[11,16,29] According to XRV data at the (0, 0, 1.3) reciprocal space position (Figure 5b), however, there is no direct correlation between this peak and the onset of surface reconstruction because at −0.15 V the surface is already half reconstructed. Rather, it should be assigned to the adsorption of OH_{ad} on the (1 × 1) phase, which begins to form as low as at −0.4 V. It has been suggested that two different types of OH_{ad} can be distinguished on the Au(100) electrode: at low potentials ($E < 0$ V), a reversible form of hydroxy species (denoted hereafter as OH_r) and, at $E > 0$ V, an irreversible oxide form of hydroxyl species (denoted hereafter as OH_{ir}). The total coverage by oxygenated species is $OH_{ad} = OH_r + OH_{ir}$. Although the exact nature of these two forms is not known, it is reasonable to postulate that the difference between the reversible and irreversible form of OH_{ad} is, in fact, the difference in coordination that these two species have with the surface Au atoms. The OH_r species formed below $E \approx 0.0$ V is adsorbed onto the outermost plane of Au atoms in a partially (or fully) discharged state. On the other hand, the OH_{ir} form is in, or below, the outermost plane of the Au atoms, the latter being formed at $E > 0.3$ V by place-exchange with Au surface atoms.[30] In the following, we show that the nature and the surface coverage of OH_{ad} species play an important role in the kinetics of the "hex" ↔ (1 × 1) transition and in the formation of the c($\sqrt{2} \times 2\sqrt{2}$)R45° structure.

The modifications to the voltammetry of Au(100) by the addition of 10^{-3} M Br in 0.1 M KOH are summarized in Figure 5a. Clearly, the presence of Br^- anions generates quite significant changes in the voltammetry curve obtained in 0.1 KOH: (i) a larger pseudocapacitance is observed between $-0.5 < E < -0.2$ V; (ii) the "reconstruction" peak appears at ≈ −0.22 V; (iii) a new peak is recorded at 0.12 V; and (iv) significant suppression of OH_{ad} adsorption is found at $E > 0$ V. All of these changes can be rationalized on the basis of the specific adsorption of Br^- anions onto Au(100). Unfortunately, the RRDE methodology cannot be utilized for the assessment of the true bromide adsorption isotherm, because at pH = 13 the Br^- conversion to Br_2 (reaction 1) overlaps with the O_2 evolution reaction.[31] However, because neither H^+ nor OH^- are involved in the adsorption step ($Br^- = Br_{ad} + e^-$), the fractional coverages of Br_{ad} should not depend on pH, so that the fractional coverages of Br_{ad} in alkaline solution should be very similar to those deduced in acid solution. Indeed, the initial adsorption of Br^-, discerned from the rising portion of the pseudocapacitance in Figure 5a, is observed at $E \approx -0.5$ V, which is close to −0.45 V found in acid solution (Figure 2b). Given that on the SCE reference scale, the surface coverage by OH_{ad} is higher in base than in acidic media, then the *competition* between Br_{ad} and OH_{ad} is pH dependent, and thus, the shape of the $E-\Theta_{Br_{ad}}$ curve may differ in these two electrolytes. The results in Figure 5b show that the decrease in the scattering intensity due to the formation of the (1 × 1) structure is shifted negatively in Br^--containing solution. Interestingly, the degree of irreversibility in the "hex" ↔ (1 × 1) transition is smaller with Br^- than without Br^-; that is, there is less hysteresis in the XRV measurements (Figure 5b). In other words, both the "hex" → (1 × 1) transition as well as the (1 × 1) → "hex" transition are enhanced by adsorption of Br_{ad}. Although the explanation of the negative shift of the equilibrium potential for the "hex" → (1 × 1) transition in the presence of bromide is straightforward, i.e., at the same potential the fractional coverages, $\Theta_{Br_{ad}} + \Theta_{OH_{ad}}$ are greater than $\Theta_{OH_{ad}}$ in solution free of Br^-, it is more difficult to rationalize the enhanced (1 × 1) → "hex" transition. A clue to this unusual behavior lies in the nature of the adsorption isotherms of Br_{ad} and OH_{ad} species and the competitive adsorption between these two adsorbates. Although the exact nature (viz. reversibility vs irreversibility) of the adsorption isotherm for OH_{ad} is unknown, it is plausible that the kinetics of the "hex" phase formation in 0.1 M KOH + 10^{-3} M Br^- are mainly controlled by *reversible* chemisorption of Br_{ad} and not by the reversible/irreversible adsorption of OH_{ad} species. This is in agreement with the substantial reduction in the fractional coverages by OH_{ad} in the presence of Br^-, which indeed is observed in Figure 5a.

Of particular interest here is the appearance of the sharp peak in the voltammetry of Figure 5a at ≈0.12 V. The position of this peak is almost the same as the peak observed in acid solution that marks the disorder−order transition of the Br_{ad} adlayer. Cosiderring that the adsorption of Br^- is pH independent, this peak might mark the formation of a c($\sqrt{2} \times 2\sqrt{2}$)-R45° superstructure with $\Theta_{Br_{ad}} = 0.5$ ML. Although a careful search was made to find diffraction peaks due to the c($\sqrt{2} \times 2\sqrt{2}$)R45° structure, no such peaks were found. It is concluded,

therefore, that a c($\sqrt{2} \times 2\sqrt{2}$)R45° structure with long-range order is not formed on the Au(100) electrode in alkaline solution. It is appropriate at this point to address the question of why it was not possible to observe scattering due to an ordered Br_{ad} adlayer structure even though the voltammetry in Figure 5a indicates that an ordered structure of Br_{ad} should be formed at 0.12 V. In line with our discussion above, the answer might be that in alkaline solution there is strong competition between Br^- and OH adsorption, and consequently, the formation of the long-range ordered c($\sqrt{2} \times 2\sqrt{2}$)R45° structure may be frustrated by the presence of coadsorbed oxygenated species. Therefore, the sharp but relatively small transition peak at 0.12 V might be the signature of the formation of a bromide adlayer with short-range order, for which the SXS diffraction peaks would be to broad and week to detect. To further probe the role of OH_{ad} in determining the bromide adlayer structure, an experiment was performed in which the coadsorbed OH_{ad} was consumed in an electrochemical reaction in which strongly adsorbed OH_{ad} is removed from the surface by a relatively weakly adsorbed reactant, in this case CO_{ad}.

3.2. Effect of CO on the Bromide *c*($\sqrt{2} \times 2\sqrt{2}$)*R*45° Structure. The effect of CO on the thermodynamics and dynamics of the "hex" Au(100) reconstruction in KOH and $HClO_4$ was previously studied by a combination of either EC−STM[29] or EC and SXS measurements.[16] It has been found that in alkaline solution CO acts to catalyze the formation of uniform "hex" domains. The explanation for this surprising behavior is that the continuous removal of OH_{ad} in the Langmuir−Hinshelwood (L−H) reaction, i.e.

$$CO_{ad} + OH_{ad} = CO_2 + H^+ + e^- \qquad (2)$$

may stabilize the "hex" phase over a much wider potential range than in CO-free alkaline solution. In acid solution, however, CO has a negligible effect on the potential range of thermodynamic stability of the "hex" ↔ (1 × 1) transition. The apparent opposite behavior observed for the "hex" ↔ (1 × 1) transition in acid versus alkaline electrolyte was rationalized on energetic grounds,[16] provided that neither specifically adsorbing anions nor OH_{ad} can be displaced by CO from the Au(100) surface, but in contrast to anions, a strongly adsorbed OH_{ad} can be oxidatively removed in the L−H reaction (eq 2) by the weakly adsorbed CO_{ad}. Consequently, although in alkaline solution the "hex" ↔ (1 × 1) transition is determined exclusively by the surface coverage of OH_{ad}, in acid solution, the equilibrium potential for this transition is controlled by the surface coverage of both OH_{ad} as well as that of specifically adsorbing anions.[16] As will be demonstrated below, the fact that CO and OH can react on the Au(100)−Br_{ad} surface determines the potential stability of the "hex" ↔ (1 × 1) transition as well as the formation of the c($\sqrt{2} \times 2\sqrt{2}$)R45° structure.

3.2.1. Acid Solution. It is now well established that specifically adsorbing anions have a big effect on the kinetics of CO oxidation. The role of anions on the kinetics of CO oxidation can be seen by comparing the polarization curve for CO oxidation on Au(100) in 0.1 M $HClO_4$ and in 0.1 M $HClO_4$ + 10^{-3} M Br^-. To ensure the complete poisoning of the electrode surface with CO prior to recording the oxidation currents, the electrode potential in saturated (1atm) solution with CO was held at −0.4 V (the immersion potential) for 5 min at a rotation rate of 1600 rpm. In Br^--free electrolyte (Figure 6a), a polarization curve for CO oxidation shows a typical "bell-like" shape; that is, a fast increase in the kinetic rate is followed first with the diffusion-limiting plateau and then by an equally fast

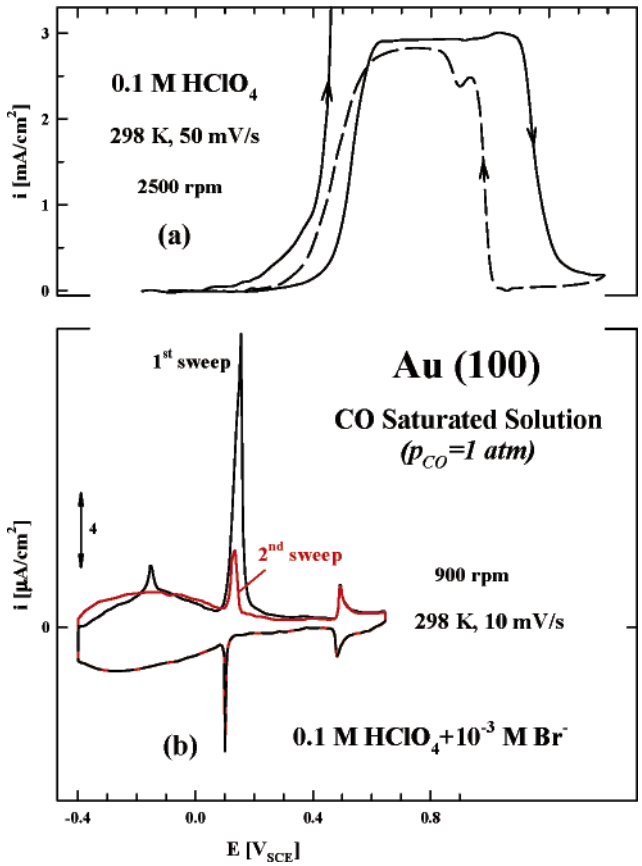

Figure 6. (a) Potentiodynamic (50 mV/s) CO oxidation current densities on Au(100) in 0.1 0.1 M $HClO_4$ saturated (1 atm) with CO under a rotation rate of 2500 rpm. To emphasise the onset of CO oxidation, also shown is the magnification of the current for CO oxidation at low overpotntials. (b) Potentiodynamic (10 mV/s) CO oxidation current densities on Au(100) in 0.1 M $HClO_4$ + 10^{-3} M Br^- saturated (1 atm) with CO under a rotation rate of 900 rpm. In the first scan (black curve), the "hex" ↔ (1 × 1) transition is seen at −0.15 V. The sharp peak at + 0.15 V corresponds to both CO oxidation as well as formation of the Br_{ad} layer. The current peak around 0.5 V is due to commensurate−incommensurate transition within the Br_{ad} adlayer. The subsequent scan in the negative direction is the same as in the CO-free solution, indicating that the L−H reaction is completely hindered by the Br_{ad} adlayer. In the second scan (red curve), the peak at 0.15 V is significantly attenuated, in agreement with a weak interaction of CO with the Au(100) surface.

deactivation. To emphasize the onset of CO oxidation, which is observed at 0.4 V, the CO currents at low potentials are magnified by a factor of 5. In solution with 10^{-3} M Br^- (Figure 6b), in the first positive sweep, a "reconstruction" peak at −0.2 V is followed first by a very sharp CO oxidation peak centered at 0.175 V (with the charge under the peak of $Q \approx 60$ $\mu C/cm^2$) and, then, above 0.2 V by a relatively small, yet readily discernible, faradic current. Note that, in acid solution containing bromide, the diffusion limiting current is not observed for CO_b oxidation even above 0.1 V, implying that Br_{ad} can effectively suppress the adsorption of OH_{ad}. In fact, close inspection of Figure 6b clearly shows that in the presence of Br^- bulk oxidation of CO is more similar to the stripping voltammetry of CO_{ad} than to the characteristic polarization curves for CO_b oxidation observed in 0.1 M $HClO_4$ (Figure 6a). On the reverse sweep, the shape of the "polarization curve" for CO oxidation is almost identical with the voltammetry recorded in CO-free solution, confirming that at positive potentials CO cannot displace chemisorbed bromide and that Br^- can effectively compete with OH^- for active surface sites. That the

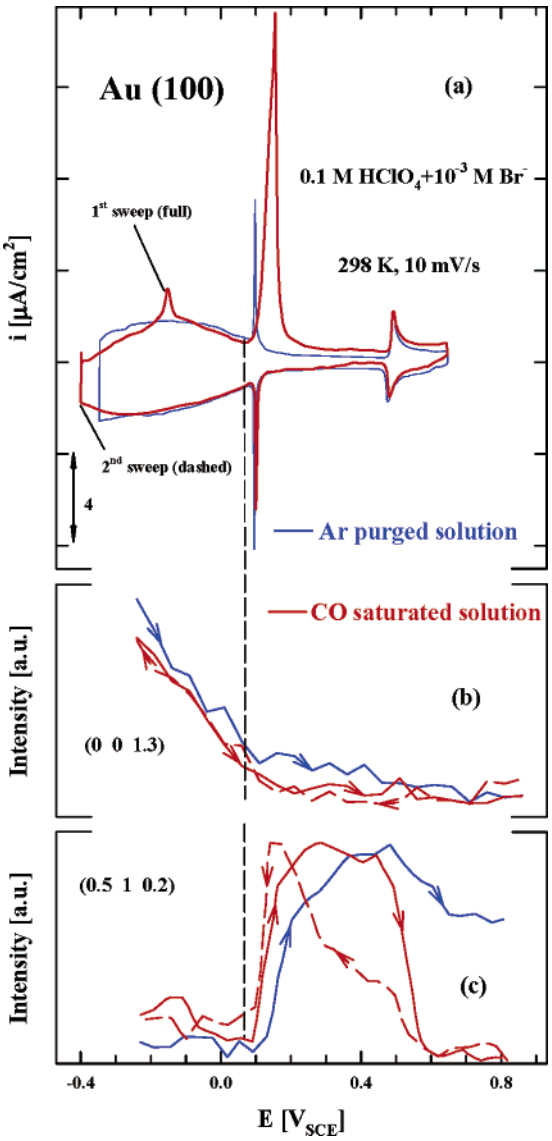

Figure 7. (a) Current−potential curves (first scan) for Au(100) in 0.1 M $HClO_4$ + 10^{-3} M Br^- purged either with argon (blue curve) or CO (red curve) at 10 mV/s. (b) Corresponding XRV measurements (2 mV/s) at (0, 0, 1.3), a position on the specular CTR; (c) XRV measurements (2 mV/s) at (0.5, 1, 0.2) where scattering from the c($\sqrt{2} \times 2\sqrt{2}$)R45° structure of Br_{ad} is observed.

Au(100)−CO interaction is weak is also supported by the second consecutive sweep of CO oxidation in Figure 6b; that is, CO oxidation is characterized first by a small peak centered at 0.15 V and then by an even smaller faradic current. On the basis of this macroscopic information, it appears that in acid solution the strength of the interaction of CO, OH^-, and Br^- with Au(100) increases in the order Au(100)−CO ≪ Au(100)−OH_{ad} < Au(100)−Br_{ad}.

Figure 7 summarizes a complementary EC−SXS examination of the surface processes at the Au(100) surface in 0.1 M $HClO_4$ + 10^{-3} M Br^- solution saturated with CO. As in our previous article,[16] microscopic insight into the structure at the Au(100) interface in the presence of CO and Br^- in 0.1 M $HClO_4$ is obtained from SXS measurements. For example, Figure 7b shows that in the presence of CO the "hex" ↔ (1 × 1) transition is shifted *negatively* by ≈40 mV. This small CO effect can be explained on the basis of a small increase in the equilibrium Br_{ad} surface coverage, which is induced by the oxidative removal of an equivalent amount of OH_{ad} in the L−H reaction, relative

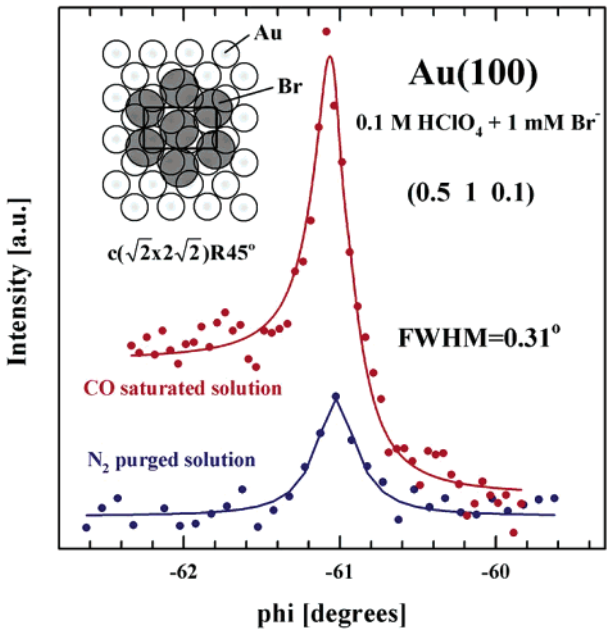

Figure 8. Rocking scans through the (0.5, 1, 0.2) reciprocal lattice position measured at 0.4 V in the absence of CO (blue curve) and in the presence of CO (red curve), where scattering from the commensurate c($\sqrt{2} \times 2\sqrt{2}$)R45° structure of the Br_{ad} adlayer in 0.1 M $HClO_4$ + 10^{-3} M Br^- is observed. The solid lines are fits of a Lorentzian line shape to the data which gives coherent domain size for the c($\sqrt{2} \times 2\sqrt{2}$)R45° structure of 150 Å. Also shown is a schematic picture of the c($\sqrt{2} \times 2\sqrt{2}$)R45° unite cell.

to that established at the same potential but in CO-free solution. Although the increase in $\Theta_{Br_{ad}}$ and the shift of the "hex" ↔ (1 × 1) transition in solution saturated with CO is rather small, adsorption of CO has a significant effect on ordering of the c($\sqrt{2} \times 2\sqrt{2}$)R45° structure. Rocking curves through the (0.5, 1, 0.1) reflection measured at 0.4 V in the absence and in the presence of CO are shown in Figure 8. The solid lines are fitted by a Lorentzian line shape to the data. Clearly, in the presence of Br^-, the c($\sqrt{2} \times 2\sqrt{2}$)R45° structure is enhanced; that is, although the domain size of the structure in both cases is ≈150 Å, in solution saturated with CO, the integrated intensity increases implying that the amount of the Au surface covered by ordered Br_{ad} has increased. The potential range of stability of the c($\sqrt{2} \times 2\sqrt{2}$)R45° structure was studied by monitoring the scattering signal at the (0.5 1 0.2) position as a function of potential. As shown in Figure 7c, in the presence of CO, the onset of formation of the commensurate c($\sqrt{2} \times 2\sqrt{2}$)R45° structure is shifted negatively by ≈40 mV, equal to the value of the thermodynamic potential shift of the "hex" ↔ (1 × 1) transition in Figure 7b, reflecting that the complete transition of the "hex" phase into the (1 × 1) phase is required in order to form the c($\sqrt{2} \times 2\sqrt{2}$)R45° structure. Further inspection of Figure 7c reveals that in the presence of CO the c($\sqrt{2} \times 2\sqrt{2}$)-R45° structure develops/disappears more rapidly than in a solution free of CO; that is, comparison of the XRV data shows that both the disorder−order transition and the commensurate−incommensurate transition are much sharper in the presence of CO at this sweep rate (2 mV/s). The observed effects of CO on both the thermodynamics as well as the dynamics of the formation of the c($\sqrt{2} \times 2\sqrt{2}$)R45° structure can be rationalized on the basis of the Au(100)-adsorbate energetics and the mutual interaction among coadsorbed species. Thus, for example, at the same electrode potential, the number of active sites for Br^- adsorption may increase in CO-saturated solution because the competing OH_{ad} species are removed from the surface in the

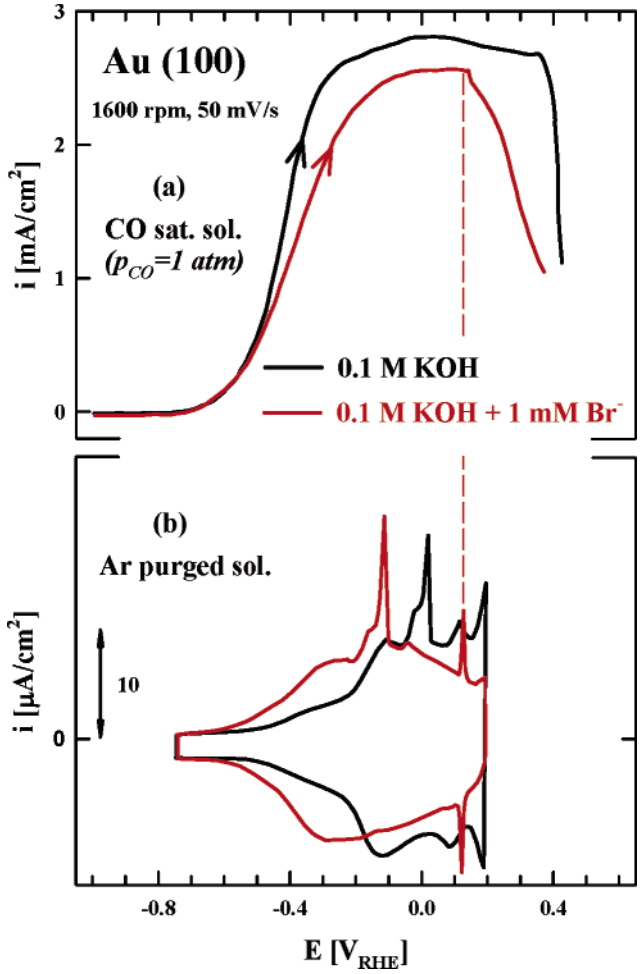

Figure 9. (a) Potentiodynamic (50 mV/s) CO oxidation current densities on Au(100) in 0.1 M KOH (black curve) and 0.1 M KOH + 10^{-3} M Br^- (red curve) under a rotation rate of 1600 rpm. (b) Cyclic voltammograms for Au(100) in argon purged 0.1 M KOH (black curve) and 0.1 M KOH + 10^{-3} M Br^- (blue curve), depicted in Figure 5, are also shown to emphasis that deactivation in the rate of CO oxidation current coincides with the formation of a sharp peak at 0.12 V, which may mark the formation of the commensurate c($\sqrt{2} \times 2\sqrt{2}$)R45° structure.

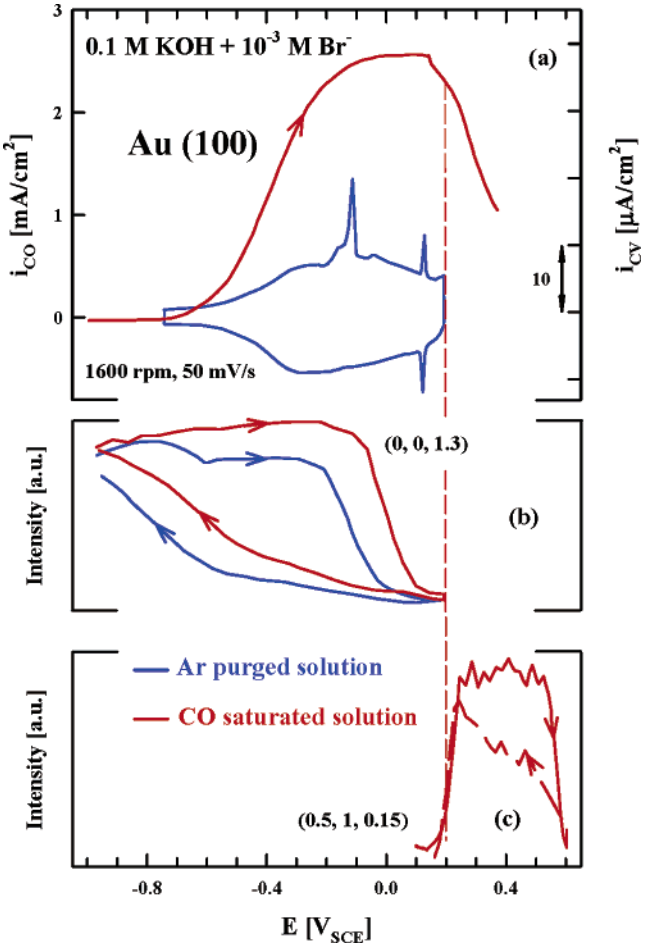

Figure 10. (a) Current potential curves for Au(100) in argon purged 0.1 M KOH + 10^{-3} M Br^- (blue curve) and in 0.1 M KOH + 10^{-3} M Br^- saturated with CO (red curve) at 50 mV/s and under a rotation rate of 1600 rpm. (b) Corresponding XRV measurements (2 mV/s) at the (0, 0, 1.3) position and (c) at the (0.5, 1, 0.15) position where in CO-saturated solution scattering from the c($\sqrt{2} \times 2\sqrt{2}$)R45° structure of Br_{ad} is observed.

L−H reaction. As a consequence, the surface coverage by Br_{ad} required to form the c($\sqrt{2} \times 2\sqrt{2}$)R45° order adlayer ($\Theta_{Br_{ad}} = 0.5$ ML) may be established at lower potentials in the presence of CO. Such a mechanism would correlate nicely with the weak adsorption of CO on Au surfaces,[32,33] i.e., that the Au(100)−Br_{ad} and Au(100)−OH_{ad} interaction is much stronger than the Au(100)−CO interaction and that only Br_{ad} and OH_{ad} are competing for the surface sites.

3.2.2. Alkaline Solution. The importance of a competitive adsorption process between Br_{ad} and OH_{ad} in the formation of an ordered structure of Br_{ad} is even more obvious in alkaline solution. In contrast to acid solution, the onset of CO oxidation on Au(100) in 0.1 M KOH is observed at relatively low potentials, from Figure 9a at ≈ −0.7 V. The fact that the rate of CO oxidation is much faster in alkaline than in acid solution is in agreement with our previous suggestion that the kinetics of the L−H reaction in acid media are not governed only by the surface concentration of CO and OH_{ad} but are also strongly affected by the delicate balance between the coverage of CO, OH_{ad}, and a third (spectator) species, viz. the anions from supporting electrolytes. This suggestion is also consistent with the results for CO electrooxidation in 0.1 M KOH +10^{-3} M Br^- solution. In agreement with our previous results, the onset of CO oxidation on Au(100) in KOH coincides with the formation of an OH_{ad} adlayer, which in Figure 9a starts at −0.3 V. At more positive potentials, the rate of CO oxidation increases sharply, reaching a diffusion-limited value at −0.1 V. Above 0.0 V, however, the current is attenuated due to significant formation of an irreversible form (not reactive) of OH_{ad}. Further inspection of Figure 9a reveals that with the addition of Br^- the current density at $E > 0.1$ V never reaches a diffusion limiting current. Given that under the same experimental conditions the rate of CO oxidation was significantly inhibited in acid solution (Figure 6a), it is reasonable to suggest that competitive adsorption between Br^- and OH^- in KOH and $HClO_4$ is rather different, i.e., OH^- adsorption in alkaline solution is more competitive with Br^- adsorption than in acid solution.

If Br_{ad} cannot be displaced by CO but OH can be oxidatively removed from the surface, then the thermodynamic potential for the Au(100) "hex" → (1 × 1) transition should be affected more in alkaline than acid solution, simply because at the same potential the Au(100) surface is more covered by OH_{ad} in the former electrolyte. Indeed, parallel electrochemical (Figure 10a) and SXS (Figure 10b) measurements in 0.1 KOH + 10^{-3} M Br^- show that, in contrast to acid solutions, in Br^- containing electrolyte the adsorbed CO promotes the potential range of stability of the "hex" phase; i.e., the "hex" → (1 × 1) transition

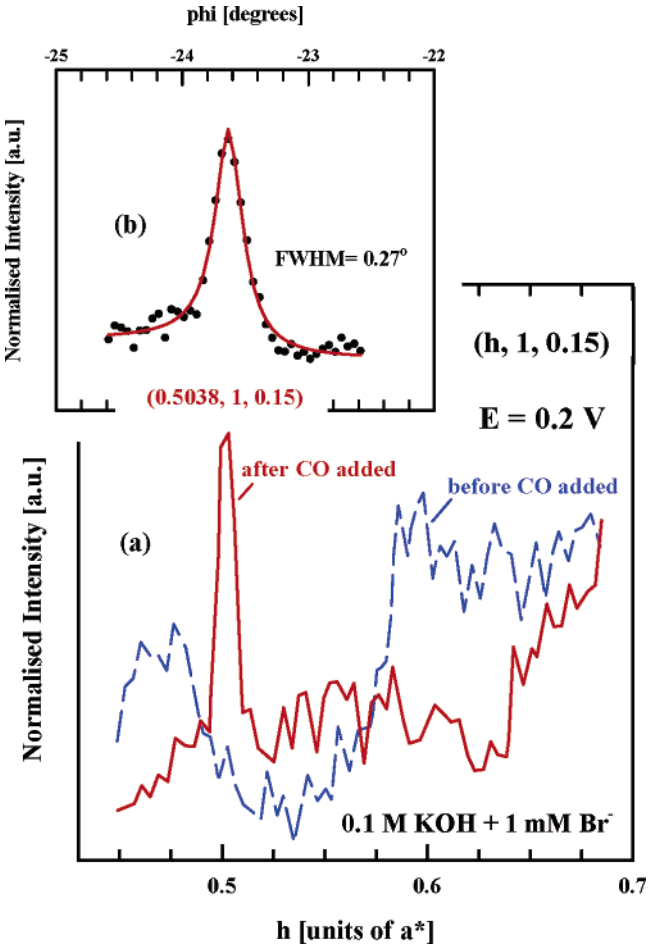

Figure 11. *h* scans through the (1/2, 1, 0.15) position before (blue curve) and after (red curve) saturating 0.1 M $HClO_4$ + 10^{-3} M Br^- solution with CO. (Insert) Rocking scans through the (1/2, 1, 0.15) reciprocal lattice position, where scattering from the commensurate c($\sqrt{2} \times 2\sqrt{2}$)R45° structure of the Br_{ad} adlayer is observed. Note, the peak is only observed in the CO-saturated solution. The solid lines are fits of a Lorentzian line shape to the data which gives coherent domain size for the c($\sqrt{2} \times 2\sqrt{2}$)R45° structure around ≈175 Å.

is shifted in the positive direction by ca. 0.12 V. In the previous SXS study, it was also found that adsorbed CO on Au(100) in alkaline solution can alter both the potential-dependent thermodynamics (shifts the "hex" ↔ (1 × 1) transition positively) as well as the dynamics (the "hex" phase develops more rapidly) of the Au(100) reconstruction.[16] Closely following the discussion in ref 16, it is reasonable to conclude that the shift in the equilibrium potential for the Au(100) "hex" ↔ (1 × 1) transition in CO saturated 0.1 M KOH + 10^{-3} M Br^- (Figure 10b) solution is induced by continuous removal of OH_{ad} in the L−H reaction.

The proposed effect of CO on competitive adsorption between Br^- and OH^- is further examined in the SXS measurements. In particular, one may expect that the removal of OH_{ad} from the Au(100) surface by weakly adsorbed CO may allow the Br_{ad} adlayer to order, as it does in acid solution. To probe the CO effect on the ordering of the Br_{ad} adlayer, an "h" scan through the (1/2, 1, 0.15) peak due to the c($\sqrt{2} \times 2\sqrt{2}$)R45° structure was measured at 0.2 V, before and after saturating the solution with CO and these scans are shown in Figure 11. Although in the absence of CO no ordered structure with the c($\sqrt{2} \times$ p)R45° symmetry is observed, in the presence of CO, a sharp peak is found at the commensurate position ($h = 0.5$). The insert of Figure 11 shows a rocking scan through this position. From the Lorentzian line shape fit (solid line) to these data, a domain size of ≈175 Å is calculated, which is close to the domain size measured in acid solution. The potential dependence of the X-ray intensity at the (1/2, 1, 0.15) position, shown in Figure 10c, reveals that fast development of the c($\sqrt{2} \times 2\sqrt{2}$)R45° structure at 0.15 V is followed by a potential window were this structure is stable (ca. 0.3 V) and finally by the third potential region where the commensurate structure disappears as fast as it is formed at 0.15 V. As in acid solution, *h* scans, such as that shown in Figure 11, show a peak due to the presence of the incommensurate c($\sqrt{2} \times$ p)R45° phase, and this peak shifts to higher *h* values as the potential is increased. On the reverse sweep, a relatively small hysteresis is observed even with the fast potential sweep rate (2 mV/s) used in our SXS experiments, indicating that in the presence of CO the commensurate−incommensurate transition is as reversible as in acid solution (see Figure 3c). In lines with the CTRs data, it appears that the ordering of the Br_{ad} adlayer in alkaline solution saturated with CO arises due to continuous removal of OH_{ad} in the L−H reaction. The turnover rate (defined as number of complete reaction events per active sites per second) of this reaction is rather low in the potential range of stability of the c($\sqrt{2} \times 2\sqrt{2}$)R45°structure ($E > 0.15$ V, as seen from Figure 10a), and thus, no significant change of pH (not during the duration of our experiment) is expected to occur in SXS experiments. This becomes even more evident if we recall that the "hex" → (1 × 1) transition in CO saturated 0.1 M KOH + 10^{-3} M Br^- is shifted in the positive (Figure 10) rater than in the negative direction, the latter being characteristic for acidic media (see Figure 3b).

Returning to the relationship between the transition peak observed in the cyclic voltammetry at 0.12 V and the domain size of the c($\sqrt{2} \times 2\sqrt{2}$)R45° structure discussed in section 3.2.2, it is apparent that the voltammetric peak at 0.12 V is indeed a fingerprint for the ordering of the Br_{ad} adlayer. Due to the strong competition between Br_{ad} and OH_{ad} in alkaline solution, however, the domain size of c($\sqrt{2} \times 2\sqrt{2}$)R45° structure is probably not large enough for a peak to be detected by SXS measurements. Perhaps utilizing scanning tunneling microscopy, which is a local probe of atomic structure, it would be possible to confirm the existence of the c($\sqrt{2} \times 2\sqrt{2}$)R45° structure of Br_{ad}, even in CO-free alkaline solution. Nevertheless, the competitive adsorption between halide anions and oxygenated species may also play a significant role in the continuous transition from the commensurate c($\sqrt{2} \times 2\sqrt{2}$)R45° structure to the incommensurate c($\sqrt{2} \times$ p)R45° structure.[13] Although a detailed understanding of the role of OH_{ad} on this phase transition in the Br_{ad} adlayer is not yet possible, the present discussion suggests that Br_{ad} compressibility may be determined not only by the adsorbate−adsorbate interaction[13,14] but in addition by strong competition for Au adsorption sites between Br_{ad} and OH_{ad}.

4. Conclusions

The surface reconstruction of Au(100) and the formation of a commensurate c($\sqrt{2} \times 2\sqrt{2}$)R45° structure of the Br adlayer have been studied by a combination of electrochemical (EC) and surface X-ray scattering (SXS) measurements. Emphasis is placed on linking the microscopic structural information regarding the Br_{ad} adlayer to the voltammetric and other macroscopic electrochemical responses, including using the rotating ring disk electrode (RRDE) technique for determining the fractional surface coverages by Br_{ad}. The RRDE ring-shielding measurements showed that the $E-\Theta_{Br_{ad}}$ curve exhibits

the "S" shape; that is, initially the bromide surface concentration changes only slowly with potential then a steep rise in coverage is observed, followed by a third regime of slow increase where the adlayer packing density is close to saturation (0.62 ML). When EC and SXS measurements are combined. it is found that relatively low Br_{ad} coverages ($\Theta_{Br_{ad}} \approx 0.1$ ML) are sufficient to trigger the lifting of the surface reconstruction. Complete lifting of the reconstruction is observed for $\Theta_{Br_{ad}} \approx 0.5$ ML, just at the potential where an ordered c($\sqrt{2} \times 2\sqrt{2}$)R45° Br^- structure is formed in acid solution. The potential range of stability of the c($\sqrt{2} \times 2\sqrt{2}$)R45° structure in acid solution is ca. 0.3 V. An incommensurate c($\sqrt{2} \times$ p)R45° phase ($0.57 < \Theta_{Br_{ad}} < 0.62$ ML) is obtained between 0.5 and 0.7 V. No ordered structures of Br^- were observed in alkaline solution although the adsorption of Br is a pH-independent process. We suggest that due to strong competition between Br^- and OH^- for adsorption sites the formation of a c($\sqrt{2} \times 2\sqrt{2}$)R45° structure with long-range order in alkaline solution may be frustrated by the presence of coadsorbed oxygenated species.

To probe the role of OH_{ad} on the formation of the ordered bromide adlayer structure, coadsorbed OH_{ad} was consumed in an electrochemical reaction in which strongly adsorbed OH_{ad} was removed from the surface by a relatively weakly adsorbed reactant, namely CO_{ad}. Under such experimental conditions, in acid solution, the c($\sqrt{2} \times 2\sqrt{2}$)R45° structure develops/disappears more rapidly in the presence of CO than in solution free of CO. In alkaline solution saturated with CO, the c($\sqrt{2} \times 2\sqrt{2}$)R45° structure is observed in exactly the same potential region as in acid solution. We propose that the continuous removal of OH_{ad} in the Langmuir-Hinhselwood reaction $CO + OH = CO_2 + H^+ + e^-$ may stabilize the c($\sqrt{2} \times 2\sqrt{2}$)R45° structure in both acid as well as alkaline media.

Acknowledgment. This work was supported by the Director, Office of Science, Office of Basic Energy Sciences, Division of Materials Sciences, U.S. Department of Energy under Contract No. DE-AC03-76SF00098. C.A.L. acknowledges the support of an EPSRC Advanced Research Fellowship, and M.E.G. acknowledges the support of an EPSRC studentship. The SXS measurements were performed at SSRL which is funded by the Division of Chemical Sciences (DCS), US DOE.

References and Notes

(1) Kolb, D. M. *Prog. Surf. Sci.* **1996**, *51*, 109−173.
(2) Markovic, N. M.; Ross, P. N. *Surf. Sci. Rep.* **2002**, *45*, 121−254.
(3) Magnussen, O. M. *Chem. Rev.* **2002**, *102*, 679−725.
(4) Lucas, C. A.; Markovic, N. M. *Encyclopedia of Electrochemistry*, section 4.1.2.1.2; Wiley-VCH: New York, 2003.
(5) Lipkowski, J.; Shi, Z.; Chen, A.; Pettinger, B.; Bilger, C. *Electrochim. Acta* **1998**, *43*, 2875−2888.
(6) Itaya, K. *Prog. Surf. Sci.* **1998**, *58*, 121−247.
(7) Gao, X.; Edens, G. J.; Weaver, M. J. *J. Phys. Chem.* **1994**, *98*, 8074−8085.
(8) Zou, S.; Gao, X.; Weaver, M. J. *Surf. Sci.* **2000**, *452*, 44−57.
(9) Cuesta, A.; Kolb, D. M. *Surf. Sci.* **2003**, *465*, 310−316.
(10) Ocko, B. M.; Wang, J.; Davenport, A.; Isaacs, H. *Phys. Rev. Lett.* **1990**, *65*, 1466−1469.
(11) Tidswell, I. M.; Markovic, N. M.; Lucas, C.; Ross, P. N. *Phys. Rev. B* **1993**, *47*, 16542.
(12) Ocko, B. M.; Magnussen, O. M.; Wang, J. X.; Adzic, R. R.; Wandlowski, T. *Physica B* **1996**, *221*, 238−244.
(13) Wandlowski, T.; Wang, J. X.; Magnussen, O. M.; Ocko, B. M. *J. Phys. Chem.* **1996**, *100*, 10277−10287.
(14) Ocko, B. M.; Magnussen, O. M.; Wang, J. X.; Wandlowski, T. *Phys. Rev. B* **2003**, *53*, 7654−7657.
(15) Magnussen, O. M.; Ocko, B. M.; Wang, J. X.; Adzic, R. R. *J. Phys. Chem.* **1996**, *100*, 550−5508.
(16) Blizanac, B. B.; Lucas, C.; Gallagher, M.; Arenz, M.; Ross, P. N.; Markovic, N. M. *J. Phys. Chem. B* **2003**, *108*, 625−634.
(17) Magnussen, O. M.; Ocko, B. M.; Adzic, R. R.; Wang, J. X. *Phys. Rev. B* **1995**, *51*, 5510−5513.
(18) Schmidt, T. J.; Stamenkovic, V.; Arenz, M.; Markovic, N. M.; Ross, P. N. *Electrochim. Acta* **2002**, *47*, 3765−3776.
(19) Gasteiger, H. A.; Markovic, N. M.; Ross, P. N. *Langmuir* **1996**, *12*, 1414−1418.
(20) Lucas, C.; Markovic, N. M.; Ross, P. N. *Surf. Sci.* **1996**, *340*, L949-L954.
(21) Lucas, C.; Markovic, N. M.; Ross, P. N. *Phys. Rev. Lett.* **1996**, *77*, 4922−4925.
(22) Lucas, C. A.; Markovic, N. M.; Grgur, B. N.; Ross, P. N. *Surf. Sci.* **2000**, *448*, 65−76.
(23) Pajkossy, T.; Wandlowski, T.; Kolb, D. M. *J. Electroanal. Chem.* **1996**, *414*, 209−220.
(24) Markovic, N. M.; Lucas, C. A.; Gasteiger, H. A.; Ross, P. N. *Surf. Sci.* **1996**, *365*, 229−240.
(25) Wandlowski, T.; Wang, J. X.; Ocko, B. M. *J. Electroanal. Chem.* **2001**, *500*, 418−434.
(26) Li, N.; Lipkowski, J. *J. Electroanal. Chem.* **2001**, *491*, 95−102.
(27) Foresti, M. L.; Innocenti, M.; Forni, F.; Guidelli, R. *Langmuir* **1998**, *14*, 7008−7016.
(28) Lei, H.-W.; Uchida, H.; Watanabe, M. *Langmuir* **1997**, *13*, 3523−3528.
(29) Edens, G. J.; Gao, X.; Weaver, M. J.; Markovic, N. M.; Ross, P. N. *Surf. Sci. Lett.* **1994**, *302*, L275−L282.
(30) Conway, B. E. *Prog. Surf. Sci.* **1995**, *49*, 331−452.
(31) Pourbaix, M. *Atlas of electrochemical equilibria in aqueous solutions*; Pergamon Press: London, 1966; p 108.
(32) Somorjai, G. A. *Introduction to Surface Chemistry and Catalysis*; John Wiley & Sons: New York, 1993.
(33) Gottfried, J. M.; Schmidt, K. J.; Schroeder, S. L. M.; Christmann, K. *Surf. Sci.* **2003**, *536*, 206−224.